Plasmodium falciparum vacuolar pyrophosphatase 1 for ring stage development and its transition to trophozoite

Omobukola Solebo[1], Liqin Ling[1,2], Jing Zhou[2], Tian-Min Fu[3,4], Hangjun Ke[1,*]

Running title: PfVP1 in *Plasmodium falciparum*

[1]Center for Molecular Parasitology, Department of Microbiology and Immunology, Drexel University College of Medicine, Philadelphia, Pennsylvania, USA

[2]Department of Laboratory Medicine, West China Hospital, Sichuan University, Chengdu, China

[3]Department of Biological Chemistry and Pharmacology, The Ohio State University College of Medicine, Columbus, OH 43210

[4]The Comprehensive Cancer Center, The Ohio State University, Columbus, OH 43210

*Correspondence: hk84@drexel.edu

Abstract

The malaria parasite relies on anaerobic glycolysis for energy supply when growing inside RBCs as its mitochondrion does not produce ATP. The ring stage lasts ~ 20 hours and is traditionally thought to be metabolically quiescent. However, recent studies show that the ring stage is active for several energy-costly processes including gene transcription/translation, protein export, and movement inside the RBC. It has remained unclear if a low glycolytic flux can meet the energy demand of the ring stage. Here we show that the metabolic by-product, pyrophosphate, is a critical energy source for the development of the ring stage and its transition to the trophozoite stage. During early phases of the asexual development, the parasite utilizes PfVP1 (*Plasmodium falciparum* vacuolar pyrophosphatase 1), an ancient pyrophosphate-driven proton pump, to pump protons across the parasite plasma membrane to maintain the membrane potential and cytosolic pH. Conditional deletion of PfVP1 leads to delayed ring stage development and a complete blockage of the ring-to-trophozoite transition, which can be partially rescued by *Arabidopsis thaliana* vacuolar pyrophosphatase 1, but not by the soluble pyrophosphatase from *Saccharomyces cerevisiae*. Proton-pumping pyrophosphatases are absent in humans, which highlights the possibility of developing highly selective VP1 inhibitors against the malaria parasite.

Introduction

Malaria is a threat to 40% of the world's population and claims nearly half a million lives each year[1]. In a human host, the malaria parasite grows exponentially in bloodstream RBCs, causing all clinical symptoms including death in severe cases. In *Plasmodium falciparum*, the 48 h Intraerythrocytic Development Cycle (IDC) can be divided into three major developmental stages, including the ring, the trophozoite, and the schizont. These stages take about ~ 22h, ~ 18h, and ~ 8h, respectively. Within the RBC, the parasite resides in a vacuole and is surrounded by three membranes: parasite plasma membrane (PPM), the parasitophorous vacuolar membrane (PVM), and the RBC membrane (RBCM). A major task of the ring stage parasite is to export proteins to the host cell to increase its permeability and cytoadherence[2]. Over the ~ 22 h period, however, the parasite is not replicating DNA or expanding its biomass significantly. After the RBCM has been permeabilized by the Plasmodium Surface Anion Channel (PSAC)[3], or New Permeability Pathways (NPPs)[4], the trophozoite stage parasite starts to grow rapidly, resulting in 16-32 progeny in the schizont stage.

It has been long recognized that the asexual stage parasites rely on anaerobic glycolysis for ATP production[5,6]. Per glucose consumed, the parasite makes 2 ATP and 2 lactate molecules, with a minimal number of glucose-derived carbons fed into the tricarboxylic acid cycle (TCA)[7]. Indeed, the parasite can tolerate deletions of many TCA cycle enzymes[7] and some components of the mitochondrial electron transport chain[8,9], implying that the mitochondrion is a negligible source of ATP in blood stages. To overcome the energy constrain mediated by substrate-level phosphorylation, the trophozoite stage parasite runs a high rate of glycolysis and consumes glucose in a rate that is 100-times faster than normal RBCs[10]. Permeabilization of the RBCM in this stage also facilitates lactate disposal to avoid a metabolic blockage of glycolysis. With an intact RBCM, however, the ring stage is traditionally thought to be metabolically quiescent, with a low-level of glycolysis being sufficient to meet the energy demand of this stage[11].

Recent studies, however, suggest that the ring stage parasite fulfills many energy-costly processes over the 22 h period. Although the genome is not replicating at this stage, RNA transcription and protein translation are active to form a ring stage specific proteome for all necessary activities[12]. The PTEX translocon catalyzes ATP hydrolysis to move hundreds of parasite proteins to the RBC cytosol and membrane throughout the ring stage[13]. Rather than being static, ring stage parasites undergo dynamic movement inside the RBC and display morphological changes between the classical ring and a deformable ameboid-like structure[14]. In addition, the ring stage parasite must spend energy to pump protons across the parasite plasma membrane to maintain the plasma membrane potential (Δψ). It has been shown that the ATP-consuming V-type ATPase is the major proton pump in trophozoite stage parasites[15]. However, no studies have been carried out to show how plasma membrane potential is maintained in ring stages. RNA-seq data suggest that subunits of V-type ATPase are not highly transcribed until the trophozoite stage[16] (and **Figure S1)**. Thus, it remains unknown how the ring stage parasite pumps protons and meets its energy demand while running a low-level of glycolysis.

In this study, we discover that the ATP independent, proton pumping pyrophosphatase PfVP1 (*Plasmodium falciparum* vacuolar pyrophosphatase 1), is the major proton pump during ring stage development. Proton-pumping pyrophosphatases, or H^+-PPases, catalyze the hydrolysis of inorganic pyrophosphate (PPi), a by-product of over 200 cellular reactions, while harnessing the energy to pump protons across a biological membrane[17]. H^+-PPase was first discovered in the plant tonoplast and was also named vacuolar pyrophosphatase[18]. While H^+-PPases are absent in fungi and metazoans, it has been evolutionally conserved in bacteria, archaea, plants, and many protozoans[19]. The *P. falciparum* genome encodes two types of H^+-PPases, PfVP1 (PF3D7_1456800) and PfVP2 (PF3D7_1235200)[20]. PfVP1 is potassium dependent and calcium independent whereas PfVP2 is potassium independent and calcium dependent. RNA-seq data suggest PfVP2 is barely transcribed[16] (**Figure S1)**, which is consistent with its non-essential role

in the asexual stages[21]. By contrast, PfVP1 is highly expressed throughout the IDC and exhibits a peak expression in the ring stage[16] (**Figure S1)**. Our data reveal that the malaria parasite employs PfVP1 to harness energy from pyrophosphate, an ancient energy source, to support vital biological processes in the ring stage when ATP supply is relatively low.

Results

PfVP1 is mainly localized to the parasite plasma membrane (PPM)

Previous attempts of localizing vacuolar pyrophosphatases in *P. falciparum* used polyclonal antibodies raised against *Arabidopsis thaliana* vacuolar pyrophosphatase 1 (AVP1) in wildtype parasites[22], which were unable to differentiate PfVP1 from PfVP2. Therefore, to specifically localize PfVP1, we utilized the CRISPR/Cas9 system[23,24] to endogenously tag *pfvp1* with either a triple hemagglutinin (3HA) tag or a monomeric fluorescent protein (mNeonGreen) in the 3D7-PfVP2KO (knockout) parasite line[21]. Additionally, through gene editing of the endogenous copy, the tagged *pfvp1* was placed under the control of the TetR-DOZI-aptamer system for conditional expression[25] (**Figure S2**). Thus, two transgenic parasite lines were constructed, 3D7-PfVP2KO-PfVP1-3HA^{apt} and 3D7-PfVP2KO-PfVP1-mNeonGreen^{apt}. We also cloned 3D7-PfVP2KO-PfVP1-3HA^{apt} by limited dilution and obtained two pure parasite clones, B11 and G11, which were phenotypically indistinguishable (B11 was used for this study). The parasite lines were normally cultured in the presence of 250 nM anhydrotetracycline (aTc) to maintain PfVP1 expression.

The subcellular localization of PfVP1 was verified by immunofluorescence analysis (IFA), immuno-electron microscopy (immuno-EM), and live fluorescence microscopy (**Figure 1**). In the 3D7-PfVP2KO-PfVP1-3HA^{apt} line, IFA revealed clear colocalization of PfVP1 and the PVM marker, PfEXP2, throughout the 48 h IDC (**Figure 1A**). Since the PVM is permeable to protons[26], the close proximity of PfVP1 to PfEXP2 suggests PfVP1 is localized on the PPM.

Further, immuno-EM studies with the HA tagged line showed localization of PfVP1 mainly to the PPM (**Figure 1B**). Quantification of 65 random images revealed 90% of the gold particles were localized to the PPM, ~ 2% of the gold particles were localized to nucleus/ER, and ~ 8% of the gold particles were localized to the cytosol or cytosolic small membranous structures with unknown identities (**Figure S3**). No gold particles were apparently localized on the food vacuole. To further confirm this, we performed co-localization studies of PfVP1 and the food vacuole using the food vacuole marker, PfPlasmepsin II[27]. We were unable to find any parasites in which PfVP1 and PfPlasmepsin II colocalized (**Figure S4**). Thus, PfVP1 did not coincide with the food vacuole as previously thought[28]. Finally, we used live microscopy to localize PfVP1 in the 3D7-PfVP2KO-PfVP1-mNeonGreen^{apt} line. PfVP1 was clearly localized to the PPM in every stage of the IDC, including the merozoite, the ring, the trophozoite, and the schizont stages (**Figure 1C**). Together, we utilized three independent methods to show that PfVP1 is mainly localized to the PPM.

In the 3D7-PfVP2KO-PfVP1-3HA^{apt} line, we revealed PfVP1 was also highly expressed by Western blot (**Figure 1D**). A regular amount of total parasite lysate (~ 15 µg) contained an abundant amount of PfVP1, from the monomeric form of 79 kDa to large, aggregated oligomers that were not solubilized by 2% SDS. The aggregated forms agreed with the fact that PfVP1 contains 16 transmembrane helices and is highly insoluble.

Characterizing PfVP1 using the Saccharomyces cerevisiae heterologous system

To confirm PfVP1 is a PPi-dependent proton pump, we expressed PfVP1 in *S. cerevisiae*. Since the 1990s, this heterologous system[29] has been widely applied to study many VP1 orthologs from plants and Archaea[30-32]. *S. cerevisiae* does not have VP1 homologs and thus provides a robust and clean system to study exogenous VP1 proteins[29]. Importantly, isolated yeast vacuolar vesicles incorporating recombinant VP1 are suitable for testing the pump's ability to

move protons from one side of the membrane to the other. The vesicles can also be used to examine VP1's enzymatic activity. We transformed the yeast strain BJ5459[33,34], which was null for the two major vacuolar proteases, PrA and PrB, with plasmids containing a copy of synthetic codon optimized PfVP1, AVP1, or a blank control. VP1 proteins were N-terminally tagged with the localization peptide of *Trypanosoma cruzi* VP1 (the first 28 amino acids) and GFP, which facilitates VP1's localization to yeast vacuoles[35]. Yeast expression of PfVP1 and AVP1 was verified by fluorescence microscopy, which showed that the GFP signal appeared mainly on the yeast vacuoles (**Figure S5**).

We followed the established protocols[36] to isolate yeast vesicles from these three lines expressing PfVP1, AVP1, or the blank control (**Figure 2A**). In isolated yeast vesicles, a 9-Amino-6-Chloro-2-Methoxyacridine (ACMA) fluorescence quenching assay was used to assess the ability of VP1 to pump protons into their lumen (Materials and Methods). The compound's fluorescence is quenched when a pH gradient forms across the vesicle membrane. The yeast V-type ATPase, also present on the vesicles, was inhibited by Bafilomycin A1. Over time, PfVP1 possessing vesicles were able to reduce ACMA fluorescence (**Figure 2B**). The positive control AVP1 expressing vesicles also quenched ACMA, as expected, whereas the negative control vesicles bearing no H^+-PPase exhibited little effect. When Nigericin was added (a proton ionophore that abolishes transmembrane proton gradients), the quenched ACMA fluorescence was restored to its original levels (**Figure 2B**). This verified that the yeast vesicles were intact and PfVP1 and AVP1 expressing vesicles had accumulated protons inside. We also assessed PfVP1's enzymatic activity by measuring free Pi released by PPi hydrolysis (Materials and Methods). In comparison to the negative control vesicles, PfVP1 expressing vesicles produced a net of 1.24 µmoles free Pi per mg of protein per h, similar to that produced by the AVP1 vesicles (1.14 µmoles/mg/h) (**Figure 2C**). Together, using the yeast heterologous expression system, we confirmed that PfVP1 is a PPi hydrolyzing proton pump.

PfVP1 is essential for ring stage development

To investigate PfVP1's essentiality during the 48h IDC, we set up knockdown studies and examined parasite viability and morphology in the 3D7-PfVP2KO-PfVP1-3HA^{apt} line. We used two approaches to remove aTc from cultures to initiate PfVP1 knockdown. In one approach, aTc was removed from Percoll isolated schizonts. In the other, aTc was removed from synchronized ring stage parasites. When aTc was removed from schizonts, the knockdown culture did not display discernible changes in parasite morphology or parasitemia in the first IDC (**Figures 3A**). This was likely because a prolonged time (~ 48 h) was needed to knock down greater than 95% of the PfVP1 protein (**Figure S6A**). However, in the second IDC after aTc removal, the knockdown parasites then showed drastic morphological changes (**Figures 3A**). Although invasion was apparently unaffected in the absence of PfVP1 (**Figure S6B**), the parasites struggled to progress through the ring stage and failed to become an early stage trophozoite in the second IDC. From 72 to 96 h, while the parasites in aTc (+) medium progressed normally from the ring to schizont stage, the size of the knockdown parasites barely increased. It appeared that PfVP1 knockdown resulted in an extended ring stage as long as ~ 48 h. To better understand the morphological changes in the 2nd IDC after aTc removal, we examined parasite development every 4 h (**Figures 3B**). Again, PfVP1 knockdown caused delayed ring stage development and a complete blockage of the ring to trophozoite transition. At the end of the 2nd IDC, we noticed that the knockdown parasites had expanded the cytosol slightly in comparison to parasites of earlier time-points and small hemozoin particles were also visible (**Figure 3B**). However, none of the knockdown parasites showed the morphology of a normal early trophozoite stage parasite. In the absence of PfVP1, the parasites were arrested in this state for several days before lysing and was unable to finish the asexual cycle. Moreover, the blockage

of ring to trophozoite transition was also observed when the knockdown experiment was initiated from ring stage parasites (**Figure 3C**).

To examine if the arrested parasites are viable, we added aTc back to the culture after aTc was removed for 72, 84 and 96 h from schizonts. The arrested ring stage parasites were able to fully progress if aTc was given back at 72 and 84 h post knockdown (data not shown), indicating that they were viable. When aTc was added back at 96 h after knockdown, however, the arrested parasites displayed poor growth in the next IDC. Although most of them were able to progress to the trophozoite stage, many appeared sick-looking and lysed on the next day (**Figure S7**). The total parasitemia only increased marginally in the aTc addback culture (**Figure S7**). Altogether, this data clearly establish that PfVP1 is essential for ring stage development, and its absence halts the maturation of the parasites at the late ring stage.

Phenotypic characterization of the PfVP1 knockdown parasites

We next characterized the knockdown phenotypes in the 3D7-PfVP2KO-PfVP1-3HA^{apt} line. We reasoned if PfVP1 was genuinely a PPi-dependent proton pump located on the PPM, changes to cytosolic pH and PPi levels would be expected in the knockdown parasite. We used the ratiometric pH sensitive dye 2',7'-Bis-(2-Carboxyethyl)-5-(and-6)-Carboxyfluorescein, Acetoxymethyl Ester (BCECF-AM), to measure cytosolic pH following the established protocol[19]. BCECF-AM is membrane permeable and is trapped inside the parasite cytosol after its ester group is removed. We initially aimed to measure cytosolic pH at 48, 72 and 96 h after aTc removal from schizonts; however, attempts to measure pH in ring stage parasites were unsuccessful. Our experience agreed with the fact that BCECF-AM has only been reported to measure cytosolic pH in trophozoite stage parasites[19,37,38], not in the ring stage. Nonetheless, we successfully detected a decrease of cytosolic pH in the knockdown culture at 48 h post aTc removal (**Figure 4A**). Next, we measured PPi levels in the knockdown cultures using a newly

developed PPi specific sensor (Materials and Methods). At 72, 84, and 96 h post aTc removal, saponin-lysed pellets were collected, and soluble metabolites were extracted using a mild process (Materials and Methods). In each sample, the concentrations of PPi and total parasite protein were measured, and the total amount of PPi (nanomoles) was normalized to total protein (mg). We observed an increase of PPi at 84 and 96 h after aTc removal (**Figure 4B**). Together, these data not only reveal the mode of action of PfVP1 in *Plasmodium*, but also suggest that when PfVP1 is knocked down, the cytosolic proton and PPi levels increase, likely preventing parasite's transition from the ring to trophozoite stage.

We next employed a chemical-genetic approach to examine how the knockdown parasites responded to antimalarials. Starting at ring stages, we washed out aTc and set up 72h SYBR green assays with varying concentrations of aTc (10, 5, 1 and 0 nM). We used 10 nM as the highest concentration since it was sufficient to support 100% parasite growth (data not shown). Drug inhibition plots and EC_{50} values obtained with parasites grown at 10 or 5 nM aTc were similar to those found with wild type parasites. However, the PfVP1 knockdown parasites became hypersensitive to all antimalarials tested when aTc concentrations were reduced to 1 or 0 nM (**Figure 4C**). This data indicated that when PfVP1 was knocked down, the parasite was so ill that it became sensitive to extremely low concentrations of all antimalarials tested. Inhibitors against PfVP1, if available, would therefore be expected to have synergy with many antimalarials. Of note, efforts to develop H^+-PPase inhibitors have already begun by others[39].

Complementation of the knockdown parasite line with yIPP1 or AVP1

In *A. thaliana*, AVP1 acidifies the plant vacuole in conjunction with V-type ATPase. The proton pumping activity of AVP1 is not as critical as the PPi hydrolysis activity since a loss-of-function of AVP1 was rescued by the yeast inorganic pyrophosphatase (yIPP1), the soluble pyrophosphatase from *S. cerevisiae*[40]. yIPP1 has the sole function of PPi removal, with no

energy saving or proton pumping activity. Therefore, the proton pumping activity and PPi hydrolysis activity of AVP1 can be de-coupled. To test if this is also true for PfVP1, we performed a second round of transfection to complement the knockdown parasite with a copy of Myc-tagged yIPP1, AVP1 or wildtype PfVP1.

To this end, we made a new knockdown line in the D10 wildtype background, resulting D10-PfVP1-3HA^{apt} line. We transfected D10-PfVP1-3HA^{apt} parasites with plasmids bearing hDHFR for selection[41] and 3Myc-tagged yIPP1, AVP1 or PfVP1(Materials and Methods). Western blots showed that all Myc tagged copies were expressed independent of aTc, while the endogenous HA tagged PfVP1 was knocked down when aTc was removed (**Figure 5A**). As expected, fluorescence microscopy showed PfVP1 or AVP1 was localized to the PPM whereas yIPP1 was in the cytosol (**Figure 5B**). When aTc was removed from schizonts for 96 h, the knockdown parasite complemented with PfVP1-3Myc displayed normal growth like the aTc (+) control, indicating that the episomal PfVP1 fully complemented the endogenous copy (**Figure 5C**). AVP1 complementation displayed a moderate rescue with two thirds of the parasites reaching the same morphology as control parasites (late trophozoite), and one third progressing to a smaller size (early trophozoite). In contrast, yIPP1 was unable to restore parasite growth when the endogenous PfVP1 was knocked down. A quantification of various parasite morphologies in all conditions is shown in **Figure 5D**. Altogether, this data indicates 1) both PfVP1's PPi hydrolysis and proton pumping activities are essential for parasite survival, and 2) although not a 100% functional replacement, the homologous plant VP1 is able to complement VP1-deficient *Plasmodium* parasites.

Structure-guided mutagenesis studies of PfVP1

To further understand the mode of action of PfVP1, we conducted structure-guided mutagenesis studies in *P. falciparum*. All VP1 orthologs have 15-17 transmembrane helices with a molecular

mass of 70-81 kDa[19]. The crystal structure of *Vigna radiata* (mung bean) VP1 (VrVP1) was resolved in 2012[17]. At the primary sequence level, PfVP1 is highly similar to VrVP1 (49% identity and 66% similarity). The transmembrane (TM) helices are well conserved between PfVP1 and VrVP1, although the inter-domain loops display noticeable differences (**Figure 6A**). VrVP1 contains longer loops between the first three TMs. Based on the crystal structure, we computationally modeled the structure of PfVP1; the model showed a high degree of conservation to VrVP1 with deviations in some loop regions (**Figure 6B**). The substrate binding and hydrolyzing site of the modeled PfVP1 also mimics that of VrVP1[17]. At this site, all the conserved residues including 8 aspartates and 1 lysine are positioned around the substrate analog, the magnesium imidodiphosphate (MgIDP) (**Figure 6C**). The proton transfer pathway formed by TMs 5, 6, 11, 12 and 16 also appears to be structurally conserved (**Figure 6D**).

Based on these structural analyses, we chose to do alanine replacement mutagenesis of two putative substrate binding residues (D236, D461) and two residues that appear to be in the proton transfer channel and exit gate (D247, L697). Since *Plasmodium* is haploid and direct mutagenesis of essential residues would be lethal, we performed these mutagenesis studies in the D10-PfVP1-3HA^{apt} line by episomal expression of mutated alleles (Materials and Methods). The effect of mutant PfVP1 on parasite viability was assessed upon knockdown of the endogenous copy by aTc removal. Fluorescence microscopy showed all mutant PfVP1 proteins were expressed and localized to the PPM (**Figure S8A**). When the endogenous HA tagged PfVP1 was knocked down by aTc removal for 96 h, all Myc tagged PfVP1 mutant alleles were still expressed (**Figure S8B**).

The mutant PfVP1 alleles had differing abilities to rescue the knockdown phenotype (**Figure 6E**). As a control, the episomal wildtype PfVP1 copy fully rescued the knockdown parasites grown in aTc (-) medium. PfVP1 alleles with D236A and D247A mutations were unable to rescue, indicating these mutations abolished the pump's functions. The PfVP1/D461A mutation

had partial rescuing ability, but most D461A expressing parasites were unable to progress to the trophozoite stage. These results largely agreed with the results obtained with equivalent mutations in VrVP1[42]. In contrast, PfVP1 differed from VrVP1 at mutation of L697A. When this residue in VrVP1 was mutated (L749A), the pump has lost proton pumping activity, although the PPi hydrolysis activity was largely remained[43]. However, the PfVP1/L697A allele had both PPi hydrolysis and proton pumping activities to fully rescue the knockdown culture. Since L697 is located at the proton exit gate, our results indicate that PfVP1 may have some structural variation from VrVP1 at least in this location. A quantification of the rescuing ability of the various mutant PfVP1 alleles is shown in **Figure S8C**.

To explore the enzymatic and proton pumping activities of each mutant PfVP1 protein, we utilized the yeast heterologous expression system as described in **Figure 2**. We individually purified yeast vesicles bearing different codon optimized PfVP1 mutant alleles from the BJ5459 strain. Fluorescence microscopy showed all modified PfVP1 proteins were expressed and localized to the yeast vacuole (**Figure S8D**). The enzymatic assays revealed that all mutant PfVP1s, except for the L697A mutation, lacked PPi hydrolysis activity (**Figure 6F**). Likewise, only PfVP1/L697A showed proton pumping activity in the ACMA quenching assay (**Figure 6G**). Altogether, using homology modeling and yeast and parasite expression systems, we find that the substrate binding site and proton transfer pathway of PfVP1 appear to be well conserved, although the proton exit gate of PfVP1 may differ from that of the plant VP1.

Discussion

Our study has revealed that PfVP1 is highly expressed and mainly localized to the parasite plasma membrane (**Figure 1**). Using the yeast heterologous expression system, we demonstrated that PfVP1 is a PPi dependent proton pump (**Figure 2**). Our genetic data uncovered the essential role of PfVP1 in early phases of the IDC, including the ring stage and

312 the ring to trophozoite transition (**Figures 3**). Conditional deletion of PfVP1 also resulted in the
313 accumulation of protons and PPi in the parasite (**Figures 4**). Overall, our data indicate that the
314 malaria parasite utilizes the ATP-independent proton pump PfVP1 to harness energy from
315 pyrophosphate, a metabolic by-product, to establish the parasite plasma membrane potential
316 (Δψ) in the ring stage.

317 While the IDCs of different malaria parasites vary between 24-72 h, the ring stage is invariably
318 the longest period. In *P. falciparum*, the duration of the ring stage (~ 22 h) combined with the
319 transition stage from the ring to trophozoite (~2-4 h) is half of the entire IDC[14]. Inside the RBC,
320 the ring stage parasite moves, changes its shape[14], and is busy exporting hundreds of proteins
321 to the host cell[2]. Moreover, the ring stage is less susceptible to many antimalarial drugs and is
322 the only stage that displays artemisinin resistance[50]. During the transition stage from the ring to
323 trophozoite, the parasite also exhibits pronounced changes[14], including a reduction in the
324 parasite diameter, formation of several small hemozoin foci, and a transient echinocytosis of the
325 host cell (RBC membrane distortion). Despite the significance of these early phases of parasite
326 development, little is known about their cellular bioenergetics.

327 Earlier studies have shown that the ring stage parasite performs glycolysis at a much lower rate
328 compared to that of the trophozoite stage[11]. Traditionally, a low-level of glycolysis is thought to
329 be sufficient to support ring stage development. However, our study has revealed that the
330 metabolic by-product PPi serves as a critical energy source during the early phases of the IDC.
331 The free energy of PPi hydrolysis under physiological conditions is estimated to be -28.9
332 kJ/mol[43], which is close to that of ATP hydrolysis (-30.5 kJ/mol). Evolutionarily, early life forms
333 on earth used PPi as the energy source before ATP emerged[44]. The early divergent malaria
334 parasite has evolutionarily reserved the ability to use PPi as a critical energy source, especially
335 at the time when the ATP level is low. During the IDC, the malaria parasite's energy supply
336 depends on inefficient ATP production via anaerobic glycolysis as the parasite's mitochondrion

is not performing oxidative phosphorylation. Therefore, PPi becomes a significant energy supplement to the ring stage parasite where glycolysis runs at a lower rate. Future studies will focus on quantifications of ATP and PPi throughout the IDC to understand their energetic contributions to the malaria parasite.

Unlike many other eukaryotes, malaria parasites generate the plasma membrane potential (Δψ) through the transport of protons rather than sodium ions[45]. The proton gradient across the plasma membrane is also used by the parasite to perform secondary active transport to move ions, nutrients, or waste products into or out of the cell[46]. It has been long recognized that the malaria parasite possesses two different types of proton pumps, the single subunit PPi-dependent H^+-PPases[20,22] and the much faster ATP-dependent multi-subunit V-type ATPase[19]. Inhibition of the V-type ATPase by Bafilomycin A1 for 10-12 min causes a rapid drop of cytosolic pH from ~ 7.3 to ~ 6.8 in trophozoite stage parasites[19]. Therefore, the much slower proton pumps, PfVP1 and PfVP2, were thought to be insignificant or "marginal" to the parasite[46]. Alternatively, other studies have hypothesized that PfVP1 and/or PfVP2 would be critical to the parasite when energy demand is high in trophozoite stage parasites[20]. In contrast to those earlier views, our results have now recognized the significance of PfVP1 for ring stage development (PfVP2 is dispensable for asexual development[21]). Our data suggest that by using PfVP1 to fulfill proton pumping across the PPM, the ring stage parasite can divert ATP to other energy costly processes such as protein export. Therefore, for the first time, we have shown that PfVP1 is the major proton pump in *Plasmodium falciparum* during the ring stage development.

It is interesting to note that the ortholog VP1 protein in *Toxoplasma gondii* (TgVP1) displays different subcellular localization and function. TgVP1 is mainly localized to acidocalcisomes and the plant-like vacuole (PLV)[47,48] and despite phenotypic alterations, a complete knockout of TgVP1 is tolerated by the parasite[46]. In *P. falciparum*, however, the large-scale mutagenesis

survey was unable to disrupt the PfVP1 gene[49]. We have shown here that PfVP1 is essential for the ring stage development. Hence, the conserved VP1 protein has seemingly adapted to perform different functions even within the Apicomplexa phylum, to which *Toxoplasma* and *Plasmodium* belong to. Unlike blood stage malaria parasites, *Toxoplasma gondii* has a much more robust mitochondrion that is a significant ATP producer[50]. On the other hand, our study has not ruled out the possible localization of PfVP1 to acidocalcisomes in malaria parasites. In contrast to *T. gondii* where acidocalcisomes are more abundant, the presence of these organelles in *Plasmodium* remains obscure. Except for merozoites[51], the classical acidocalcisomes have not been firmly reported in other asexual stage parasites. Further investigation is needed to clarify if acidocalcisomes are present in malaria parasites and if PfVP1 is present on them.

In summary, our data suggest that the malaria parasite utilizes PfVP1 to harness energy from PPi to establish the plasma membrane potential, extrude cytosolic protons, and maintain an energy homeostasis. The essential nature of PfVP1 combined with the absence of any orthologs in humans has also highlighted it as a potential antimalarial drug target. A drug target in the ring stage is highly desired to the drug development pipeline, inhibitors of which could be partnered with many other antimalarials that kill metabolically more active stages. A combination therapy targeting both young and mature malaria parasites can then ensure all parasite forms are dispatched. Although at early stages, efforts of developing inhibitors against H^+-PPases including PfVP1 have already begun[39].

Materials and Methods

1, Plasmid construction for studies in *P. falciparum* and *S. cerevisiae* was described in Supplementary Information.

2, Parasite culture, transfection, and knockdown studies

The 3D7-PfVP2KO (PfVP2 knockout) line was generated previously[21]. We used RPMI-1640 media supplemented with Albumax I (0.5%) to culture *P. falciparum* parasites in human O^+ RBCs as previously described[41,52]. We transfected *P. falciparum* ring stage parasites (~ 5% parasitemia) either with linearized or circular plasmid (~ 50 µg) using a BioRad electroporator. Post electroporation, parasite cultures were maintained in proper drug selections, e.g., blasticidin (2.5 µg/mL, InvivoGen), WR99210 (5 nM, a kind gift from Jacobs Pharmaceutical), and anhydrotetracycline (aTc) (250 nM, Fisher Scientific). Parasite synchronization was performed with several rounds of alanine/HEPES (0.5M/10 mM) treatment. For knockdown studies, synchronized parasites were washed thrice with 1xPBS to remove aTc and diluted in fresh blood (1:10) to receive aTc (+) or (-) media.

3, Yeast culture, yeast lines and transformation

The *S. cerevisiae* strain BJ5459 was kindly supplied by Dr. Katrina Cooper from Rowan University[34], which was originally created by[33]. This strain (*MAT*a, *his3*Δ*200, can1, ura3–52, leu2*Δ*1, lys2–801, trp1-289, pep4*Δ*::HIS3, prb1*Δ*1.6R*) lacks yeast vacuolar proteases PrA (proteinase A) and PrB (proteinase B). Yeast cultures were maintained at 30ºC either in YPD or Uracil drop-out medium. YPD medium contains 1% yeast extract (BP1422-500, Fisher Scientific), 2% peptone (20-260, Genesee Scientific), and 4% dextrose. Ura drop-out medium contains uracil minus complete supplement mixture (1004-010, Sunrise Science) and dropout base powder (1650-250, Sunrise Science). The latter has yeast nitrogen base (1.7 g/L), ammonium sulfate (5 g/L) and dextrose (20 g/L). Ura drop-out solid medium contains extra 2%

407 agar. Yeast transformation was carried out using the Frozen-EZ Yeast Transformation II Kit
408 (T2001, Zymo Research), according to manufacturer's protocols.

409 4, Immunofluorescence analysis (IFA) and immuno-electron microscopy

410 IFA was carried out as previously described[41,52]. Immuno-EM was performed at the Molecular
411 Microbiology Imaging Facility at Washington University in St. Louis, MO. We used the following
412 primary antibodies and dilutions: the HA probe (mouse, sc-7392, Santa Cruz Biotechnology;
413 1:300), the Myc probe (rabbit, 2278S, Cell signaling; 1:300), PfExp2 (rabbit, a kind gift from Dr.
414 James Burns, Drexel University; 1:500), and PfPlasmepsin II (rabbit, Bei Resources, NIAID/NIH;
415 1:1000). We used fluorescently labeled secondary antibodies from Life Technologies
416 (ThermoFisher Scientific) (anti-mouse or anti-rabbit, 1:300) or goat anti-mouse 18 nm colloidal
417 gold-conjugated secondary antibody (Jackson ImmunoResearch Laboratories), as described
418 previously[52]. Other details can be found[52].

419 5, Western blot

420 Infected RBCs were lysed with 0.05% Saponin/PBS supplemented with 1x protease inhibitor
421 cocktail (Apexbio Technology LLC) and protein was extracted with 2%SDS/62 mM Tris-HCl (pH
422 6.8) as previously described[41,52]. After protein transfer, the blot was stained with 0.1% Ponceau
423 S/5% acetic acid for 5 min, de-stained by several PBS washes, and blocked with 5% non-fat
424 milk/PBS. We used the following primary antibody dilutions: the HA probe (1:10,000), the Myc
425 probe (1:8,000), and PfExp2 (1:10,000). We used HRP conjugated goat anti-mouse secondary
426 antibody (A16078, ThermoFisher Scientific) at 1:10,000 or goat anti-rabbit HRP-conjugated
427 secondary antibody (31460, ThermoFisher Scientific) at 1:10,000. Other steps followed the
428 standard BioRad Western protocols. For all Western samples, protein concentration was
429 determined using the detergent tolerant Pierce™ BCA Protein Assay Kit (23227, ThermoFisher)
430 according to the manufacturer's protocols.

6, pH measurement using BCECF-AM (2',7'-Bis-(2-Carboxyethyl)-5-(and-6)-Carboxyfluorescein, Acetoxymethyl Ester)

We measured the pH of saponin permeabilized parasitized RBCs using the pH-sensitive fluorescent dye (BCECF-AM) according to published protocols[15]. Details can be found in Supplementary Information.

7, PPi extraction and measurement

Soluble metabolites were extracted from saponin treated parasites by four rounds of freezing/thawing and mild sonication. PPi was measured using a PPi fluorogenic sensor from Abcam (ab179836). The chemical identity of this sensor was not released by the manufacturer. Details can be found in Supplementary Information.

8, SYBR Green Assays

We performed SYBR green assays as previously published[52]. Compounds used in this study included Bafilomycin A1 (NC1351384, Cayman Chemical), chloroquine (AC455240250, Fisher Scientific), atovaquone (A7986, MilliporeSigma), and artemisinin (a kind gift from Dr. Jianping Song at Guangzhou University of Chinese Medicine, China). In brief, drugs were serially diluted (3-fold) in 96 well plates in regular medium. Parasites from aTc plus culture (0.5% ring at 4% hematocrit) were washed several times with PBS and resuspended in various concentrations of aTc (20, 10, 2, or 0 nM) and incubated with diluted drugs, yielding final concentrations of aTc at 10, 5, 1, and 0 nM. Data was analyzed by GraphPad Prism6.

9, Yeast vesicle isolation

We followed published protocols to purify yeast vesicles expressing various VP1 proteins[29,36]. Details can be found in Supplementary Information.

10, ACMA pH Quenching Assay

We measured proton pumping activities of VP1 in isolated yeast vesicles using the ACMA Fluorescence Quenching Assay[36]. ACMA stands for 9-amino-6-chloro-2-methoxyacridine (A1324, ThermoFisher Scientific). For each measurement in the spectrofluorometer (Hitachi F-7000), 30 µg of vesicles were added to the 1 mL of transport buffer (100 mM KCl, 50 mM NaCl, and 20 mM HEPES) in the presence of 1 µM of ACMA, 3 mM $MgSO_4$, 1 mM of Na_2PPi and 1 µM of Bafilomycin A1 (inhibitor of the yeast V-type ATPase). The reaction was monitored for 15 minutes to observe any decrease in fluorescence (excitation 410 nm, emission 490 nm). Afterwards, 10 µM of Nigericin is added to the solution and monitored for 3 min to see if the fluorescence could be restored.

11, Pyrophosphatase activity

The release of Pi by pyrophosphatase activity of VP1 proteins in isolated yeast vesicles was measured using the P_iPer ™ Phosphatase Assay Kit (P22061, ThermoFisher Scientific), according to manufacturer's protocols. The Pi derived from PPi hydrolysis is coupled to three enzymatic reactions to convert a nonfluorescent compound (amplex red) to fluorescent resorufin. Fluorescence was detected by Tecan infinite 200 pro at 565 nm with excitation at 530 nm. A Pi standard curve was generated to determine Pi concentrations in the samples.

Figure Legend

Figure 1. PfVP1 is mainly localized to the parasite plasma membrane

A, Immunofluorescence assay of Pf3D7VP2KO-VP1-3HA. DAPI stains the nuclei. Green, PfVP1-3HA. Red, PfEXP2. Note an ameboid ring stage parasite in the first row. R, ring. T, trophozoite. S, schizont. Scale bar, 5 µm. B, Immunoelectron microscopy. RBCM, RBC membrane. PVM, parasitophorous vacuolar membrane. PPM, parasite plasma membrane. Scale bars, 200 nm. C, Live imaging of Pf3D7VP2KO-VP1-mNeonGreen. M, merozoite. R, ring. T, trophozoite. S, schizont. Scale bar, 5 µm. D, Live imaging of Percoll enriched Pf3D7VP2KO-VP1-mNeonGreen parasites. Scale bar, 10 µm. E, Western blot showing PfVP1-3HA expression. PfExp2 is the loading control.

Figure 2. PfVP1 is a PPi hydrolyzing proton pump

A, A general schematic of purifying yeast vesicles bearing VP1 proteins from *Saccharomyces cerevisiae*. Yeast cells were treated with Zymolyase to remove the cell wall, lysed by Dounce, and applied to a ficoll gradient (16% and 8%). After ultracentrifugation, yeast vesicles were collected from the top. B, ACMA quenching assay. The ACMA's fluorescence signal was recorded after the yeast vesicles were added with the substrate, Na_2PPi. Data shown are the representative of five individual experiments. C, Pyrophosphatase activity. The background activity from the negative control (NC) vesicles was subtracted from all measurements. This experiment was repeated three times with (n=3) technical replicates.

Figure 3. PfVP1 is essential for the ring to trophozoite transition

A, Knockdown experiment starting at the schizont stage. B, Parasite morphological changes throughout the time course. Green box, aTc (+). Red box, aTc (-). C. Knockdown experiment starting at the ring stage. A-C, images were Giemsa-stained thin blood smears. Bars, 5 µm. B-

C, White arrows indicate hemozoin particles. These experiments were repeated more than five times (A, C) or two times (B).

Figure 4. Phenotypic analysis of the PfVP1 knockdown parasite

A, pH measurement in the knockdown parasite after aTc removal for 48 h from the schizont stage. B, PPi measurement in the knockdown parasite. In A-B, error bars indicate variations of n=3 measurements in each condition; statistical analysis was done by Student t-test. *, $p < 0.05$. **, $p < 0.01$. ***, $p < 0.001$. C, Sensitivity to antimalarials measured by SYBR green assays. EC_{50} values were only retrievable from cultures grown in 10 or 5 nM aTc. Bafilomycin A1, 8.1 vs 7.5 nM. Chloroquine, 6.3 vs 6.4 nM. Artemisinin, 7.3 vs 10.2 nM. Atovaquone, 0.1 vs 0.15 nM. This experiment was repeated three times.

Figure 5. The dual functionality of PfVP1 is required for parasite survival

A, Western blot of complemented proteins. PfExp2 serves as a loading control. B, Immunofluorescence analysis (IFA). The complemented lines were probed with anti-Myc and a fluorescent secondary antibody. Scale bar, 5 µm. C, Morphologies of complemented parasite lines at 96 h after aTc removal. This experiment was repeated three times. D, Quantification of parasite morphologies in C. The percentage of different parasite morphological stages was determined by counting 1000 infected RBCs in each condition. R, ring. ET, early trophozoite. LT, late trophozoite. S, schizont. This experiment was repeated two times. A-D, KD means knockdown.

Figure 6. Structure guided mutagenesis analysis of PfVP1

A, 2D schematic of PfVP1 and VrVP1 containing 16 transmembrane helices (TMs). In each monomer, TMs of 5, 6, 11, 12, 15, 16 (darker) form the inner circle whereas the rest 10 TMs (lighter) form the outer circle. Protons are pumped from the cytosolic side to the luminal side. B.

Structure of PfVP1 (green) overlayed with the crystal structure of *Vigna radiate* VP1 (VrVP1, pink). The PfVP1 structure was predicted using RoseTTaFold. C. Substrate binding site of PfVP1. The side chains of substrate binding amino acids were highlighted in sticks. Magnesium ions were shown in magenta spheres. IDP stands for imidodiphosphate, which was used to co-crystalize VrVP1[17]. Boxed residues will be mutated. D. Side view of the inner circle formed by TM5, TM6, TM11, TM12 and TM16. The proton transfer pathway is located at the lower part of the inner circle. Residues subjected to mutagenesis are indicated. E, Parasite morphologies of mutated PfVP1 lines at 96 h after aTc removal from the schizont stage. Giemsa-stained smears were shown. This experiment was repeated three times. F, Pyrophosphatase activity. The background activity of negative control (NC) yeast vesicles was subtracted from all measurements. This experiment was repeated three times (n=3). G, Proton pumping activity of mutant PfVP1 alleles. Data shown are the representative of 3-5 experiments in each yeast line.

Acknowledgements

We thank members of the Ke lab, Swati Dass, Neeta Shadija, and Dr. Maruthi Mulaka, for technical assistance. We thank members of the Dr. Akhil Vaidya's lab at Drexel University for constructive discussions and Dr. Michael Mather, Ian Lamb, and Swaksha Rachuri for editing the manuscript. We thank Dr. Kendal Hirschi's lab (Baylor College of Medicine) and Dr. Katrina Cooper's lab (Rowan University) for providing yeast plasmids and strains. We thank Dr. James Burn (Drexel University), Dr. Daniel Goldberg (Washington University St Louis), and Dr. Joshua Beck (Iowa State University) for providing antibodies and plasmids. We thank Dr. Jacquin Niles (Massachusetts Institute of Technology) and Dr. Sean Prigge (Johns Hopkins University) for providing the knockdown tools. We thank Dr. Wandy Beatty (Washington University St Louis) for performing immune-EM studies. This work was supported by a Career Transition Award from NIH/NIAID (K22AI127702) and a R21 grant from NIH/NIAID (1R21AI156735) to Dr. Hangjun Ke.

Author contributions

O.S., L.L., and H.K. performed all experiments. T.M.F generated the modeled PfVP1 structures. H.K. and J.Z. designed all experiments. H.K. and O.S. wrote the manuscript, which was reviewed and edited by all other authors.

Competing interests

The authors declare no competing interests.

Data availability

All data generated in this study have been included in the manuscript and the supplementary information.

References

1 WHO. World Malaria Report. (2020).

2 Beck, J. R. & Ho, C. M. Transport mechanisms at the malaria parasite-host cell interface. *PLoS Pathog* **17**, e1009394, doi:10.1371/journal.ppat.1009394 (2021).

3 Desai, S. A., Bezrukov, S. M. & Zimmerberg, J. A voltage-dependent channel involved in nutrient uptake by red blood cells infected with the malaria parasite. *Nature* **406**, 1001-1005, doi:10.1038/35023000 (2000).

4 Ginsburg, H., Krugliak, M., Eidelman, O. & Cabantchik, Z. I. New permeability pathways induced in membranes of Plasmodium falciparum infected erythrocytes. *Mol Biochem Parasitol* **8**, 177-190, doi:10.1016/0166-6851(83)90008-7 (1983).

5 Speck, J. F., Evans, E. A. Jr. The Biochemistry of the Malaria Parasite II. Glycolysis in Cell-Free Preparations of the Malaria Parasite. *J Biol Chem* **159** (1945).

6 Sherman, I. W. Biochemistry of Plasmodium (malarial parasites). *Microbiol Rev* **43**, 453-495, doi:10.1128/mr.43.4.453-495.1979 (1979).

7 Ke, H. *et al.* Genetic investigation of tricarboxylic acid metabolism during the Plasmodium falciparum life cycle. *Cell Rep* **11**, 164-174, doi:10.1016/j.celrep.2015.03.011 (2015).

8 Ke, H. *et al.* Mitochondrial type II NADH dehydrogenase of Plasmodium falciparum (PfNDH2) is dispensable in the asexual blood stages. *PLoS One* **14**, e0214023, doi:10.1371/journal.pone.0214023 (2019).

9 Sturm, A., Mollard, V., Cozijnsen, A., Goodman, C. D. & McFadden, G. I. Mitochondrial ATP synthase is dispensable in blood-stage Plasmodium berghei rodent malaria but essential in the mosquito phase. *Proc Natl Acad Sci U S A* **112**, 10216-10223, doi:10.1073/pnas.1423959112 (2015).

10 Kirk, K. Membrane transport in the malaria-infected erythrocyte. *Physiol Rev* **81**, 495-537, doi:10.1152/physrev.2001.81.2.495 (2001).

11 Pfaller, M. A., Krogstad, D. J., Parquette, A. R. & Nguyen-Dinh, P. Plasmodium falciparum: stage-specific lactate production in synchronized cultures. *Exp Parasitol* **54**, 391-396, doi:10.1016/0014-4894(82)90048-0 (1982).

12 Bozdech, Z. *et al.* The transcriptome of the intraerythrocytic developmental cycle of Plasmodium falciparum. *PLoS Biol* **1**, E5, doi:10.1371/journal.pbio.0000005 (2003).

13 Ho, C. M. *et al.* Malaria parasite translocon structure and mechanism of effector export. *Nature* **561**, 70-75, doi:10.1038/s41586-018-0469-4 (2018).

14 Gruring, C. *et al.* Development and host cell modifications of Plasmodium falciparum blood stages in four dimensions. *Nat Commun* **2**, 165, doi:10.1038/ncomms1169 (2011).

15 Saliba, K. J. & Kirk, K. pH regulation in the intracellular malaria parasite, Plasmodium falciparum. H(+) extrusion via a V-type H(+)-ATPase. *J Biol Chem* **274**, 33213-33219, doi:10.1074/jbc.274.47.33213 (1999).

16 Bartfai, R. *et al.* H2A.Z demarcates intergenic regions of the plasmodium falciparum epigenome that are dynamically marked by H3K9ac and H3K4me3. *PLoS Pathog* **6**, e1001223, doi:10.1371/journal.ppat.1001223 (2010).

17 Lin, S. M. *et al.* Crystal structure of a membrane-embedded H+-translocating pyrophosphatase. *Nature* **484**, 399-403, doi:10.1038/nature10963 (2012).

18 Takeshige, K., Tazawa, M. & Hager, A. Characterization of the H Translocating Adenosine Triphosphatase and Pyrophosphatase of Vacuolar Membranes Isolated by Means of a Perfusion Technique from Chara corallina. *Plant Physiol* **86**, 1168-1173, doi:10.1104/pp.86.4.1168 (1988).

19 Holmes, A. O. M., Kalli, A. C. & Goldman, A. The Function of Membrane Integral Pyrophosphatases From Whole Organism to Single Molecule. *Front Mol Biosci* **6**, 132, doi:10.3389/fmolb.2019.00132 (2019).
20 McIntosh, M. T., Drozdowicz, Y. M., Laroiya, K., Rea, P. A. & Vaidya, A. B. Two classes of plant-like vacuolar-type H(+)-pyrophosphatases in malaria parasites. *Mol Biochem Parasitol* **114**, 183-195, doi:10.1016/s0166-6851(01)00251-1 (2001).
21 Ganesan, S. M. *et al.* Yeast dihydroorotate dehydrogenase as a new selectable marker for Plasmodium falciparum transfection. *Mol Biochem Parasitol* **177**, 29-34, doi:10.1016/j.molbiopara.2011.01.004 (2011).
22 Luo, S., Marchesini, N., Moreno, S. N. & Docampo, R. A plant-like vacuolar H(+)-pyrophosphatase in Plasmodium falciparum. *FEBS Lett* **460**, 217-220, doi:10.1016/s0014-5793(99)01353-8 (1999).
23 Ghorbal, M. *et al.* Genome editing in the human malaria parasite Plasmodium falciparum using the CRISPR-Cas9 system. *Nat Biotechnol* **32**, 819-821, doi:10.1038/nbt.2925 (2014).
24 Wagner, J. C., Platt, R. J., Goldfless, S. J., Zhang, F. & Niles, J. C. Efficient CRISPR-Cas9-mediated genome editing in Plasmodium falciparum. *Nat Methods* **11**, 915-918, doi:10.1038/nmeth.3063 (2014).
25 Ganesan, S. M., Falla, A., Goldfless, S. J., Nasamu, A. S. & Niles, J. C. Synthetic RNA-protein modules integrated with native translation mechanisms to control gene expression in malaria parasites. *Nat Commun* **7**, 10727, doi:10.1038/ncomms10727 (2016).
26 Desai, S. A. & Rosenberg, R. L. Pore size of the malaria parasite's nutrient channel. *Proc Natl Acad Sci U S A* **94**, 2045-2049, doi:10.1073/pnas.94.5.2045 (1997).
27 Klemba, M., Beatty, W., Gluzman, I. & Goldberg, D. E. Trafficking of plasmepsin II to the food vacuole of the malaria parasite Plasmodium falciparum. *J Cell Biol* **164**, 47-56, doi:10.1083/jcb200307147 (2004).
28 Saliba, K. J. *et al.* Acidification of the malaria parasite's digestive vacuole by a H+-ATPase and a H+-pyrophosphatase. *J Biol Chem* **278**, 5605-5612, doi:10.1074/jbc.M208648200 (2003).
29 Kim, E. J., Zhen, R. G. & Rea, P. A. Heterologous expression of plant vacuolar pyrophosphatase in yeast demonstrates sufficiency of the substrate-binding subunit for proton transport. *Proc Natl Acad Sci U S A* **91**, 6128-6132, doi:10.1073/pnas.91.13.6128 (1994).
30 Kim, E. J., Zhen, R. G. & Rea, P. A. Site-directed mutagenesis of vacuolar H(+)-pyrophosphatase. Necessity of Cys634 for inhibition by maleimides but not catalysis. *J Biol Chem* **270**, 2630-2635, doi:10.1074/jbc.270.6.2630 (1995).
31 Drozdowicz, Y. M. *et al.* A thermostable vacuolar-type membrane pyrophosphatase from the archaeon Pyrobaculum aerophilum: implications for the origins of pyrophosphate-energized pumps. *FEBS Lett* **460**, 505-512, doi:10.1016/s0014-5793(99)01404-0 (1999).
32 Van, R. C. *et al.* Role of transmembrane segment 5 of the plant vacuolar H+-pyrophosphatase. *Biochim Biophys Acta* **1709**, 84-94, doi:10.1016/j.bbabio.2005.05.011 (2005).
33 Jones, E. W., Zubenko, G. S. & Parker, R. R. PEP4 gene function is required for expression of several vacuolar hydrolases in Saccharomyces cerevisiae. *Genetics* **102**, 665-677 (1982).
34 Willis, S. D., Hanley, S. E., Beishke, T., Tati, P. D. & Cooper, K. F. Ubiquitin-proteasome-mediated cyclin C degradation promotes cell survival following nitrogen starvation. *Mol Biol Cell* **31**, 1015-1031, doi:10.1091/mbc.E19-11-0622 (2020).
35 Perez-Castineira, J. R., Hernandez, A., Drake, R. & Serrano, A. A plant proton-pumping inorganic pyrophosphatase functionally complements the vacuolar ATPase transport

activity and confers bafilomycin resistance in yeast. *Biochem J* **437**, 269-278, doi:10.1042/BJ20110447 (2011).

36 Scholz-Starke, J. *et al.* The flip side of the Arabidopsis type I proton-pumping pyrophosphatase (AVP1): Using a transmembrane H(+) gradient to synthesize pyrophosphate. *J Biol Chem* **294**, 1290-1299, doi:10.1074/jbc.RA118.006315 (2019).

37 Hayashi, M. *et al.* Vacuolar H(+)-ATPase localized in plasma membranes of malaria parasite cells, Plasmodium falciparum, is involved in regional acidification of parasitized erythrocytes. *J Biol Chem* **275**, 34353-34358, doi:10.1074/jbc.M003323200 (2000).

38 Tang, T. *et al.* Inhibitory Mechanisms of DHA/CQ on pH and Iron Homeostasis of Erythrocytic Stage Growth of Plasmodium Falciparum. *Molecules* **24**, doi:10.3390/molecules24101941 (2019).

39 Johansson, N. G. *et al.* Discovery of Membrane-Bound Pyrophosphatase Inhibitors Derived from an Isoxazole Fragment. *ACS Med Chem Lett* **11**, 605-610, doi:10.1021/acsmedchemlett.9b00537 (2020).

40 Ferjani, A. *et al.* Keep an eye on PPi: the vacuolar-type H+-pyrophosphatase regulates postgerminative development in Arabidopsis. *Plant Cell* **23**, 2895-2908, doi:10.1105/tpc.111.085415 (2011).

41 Ke, H., Dass, S., Morrisey, J. M., Mather, M. W. & Vaidya, A. B. The mitochondrial ribosomal protein L13 is critical for the structural and functional integrity of the mitochondrion in Plasmodium falciparum. *J Biol Chem* **293**, 8128-8137, doi:10.1074/jbc.RA118.002552 (2018).

42 Asaoka, M., Segami, S. & Maeshima, M. Identification of the critical residues for the function of vacuolar H(+)-pyrophosphatase by mutational analysis based on the 3D structure. *J Biochem* **156**, 333-344, doi:10.1093/jb/mvu046 (2014).

43 Frey, P. A. & Arabshahi, A. Standard free energy change for the hydrolysis of the alpha, beta-phosphoanhydride bridge in ATP. *Biochemistry* **34**, 11307-11310, doi:10.1021/bi00036a001 (1995).

44 Baykov, A. A., Malinen, A. M., Luoto, H. H. & Lahti, R. Pyrophosphate-fueled Na+ and H+ transport in prokaryotes. *Microbiol Mol Biol Rev* **77**, 267-276, doi:10.1128/MMBR.00003-13 (2013).

45 Allen, R. J. & Kirk, K. The membrane potential of the intraerythrocytic malaria parasite Plasmodium falciparum. *J Biol Chem* **279**, 11264-11272, doi:10.1074/jbc.M311110200 (2004).

46 Ginsburg, H. Abundant proton pumping in Plasmodium falciparum, but why? *Trends Parasitol* **18**, 483-486, doi:10.1016/s1471-4922(02)02350-4 (2002).

47 Miranda, K. *et al.* Characterization of a novel organelle in Toxoplasma gondii with similar composition and function to the plant vacuole. *Mol Microbiol* **76**, 1358-1375, doi:10.1111/j.1365-2958.2010.07165.x (2010).

48 Liu, J. *et al.* A vacuolar-H(+) -pyrophosphatase (TgVP1) is required for microneme secretion, host cell invasion, and extracellular survival of Toxoplasma gondii. *Mol Microbiol* **93**, 698-712, doi:10.1111/mmi.12685 (2014).

49 Zhang, M. *et al.* Uncovering the essential genes of the human malaria parasite Plasmodium falciparum by saturation mutagenesis. *Science* **360**, doi:10.1126/science.aap7847 (2018).

50 Huet, D., Rajendran, E., van Dooren, G. G. & Lourido, S. Identification of cryptic subunits from an apicomplexan ATP synthase. *Elife* **7**, doi:10.7554/eLife.38097 (2018).

51 Ruiz, F. A., Luo, S., Moreno, S. N. & Docampo, R. Polyphosphate content and fine structure of acidocalcisomes of Plasmodium falciparum. *Microsc Microanal* **10**, 563-567, doi:10.1017/S1431927604040875 (2004).

52 Ling, L. *et al.* Genetic ablation of the mitoribosome in the malaria parasite Plasmodium falciparum sensitizes it to antimalarials that target mitochondrial functions. *J Biol Chem* **295**, 7235-7248, doi:10.1074/jbc.RA120.012646 (2020).

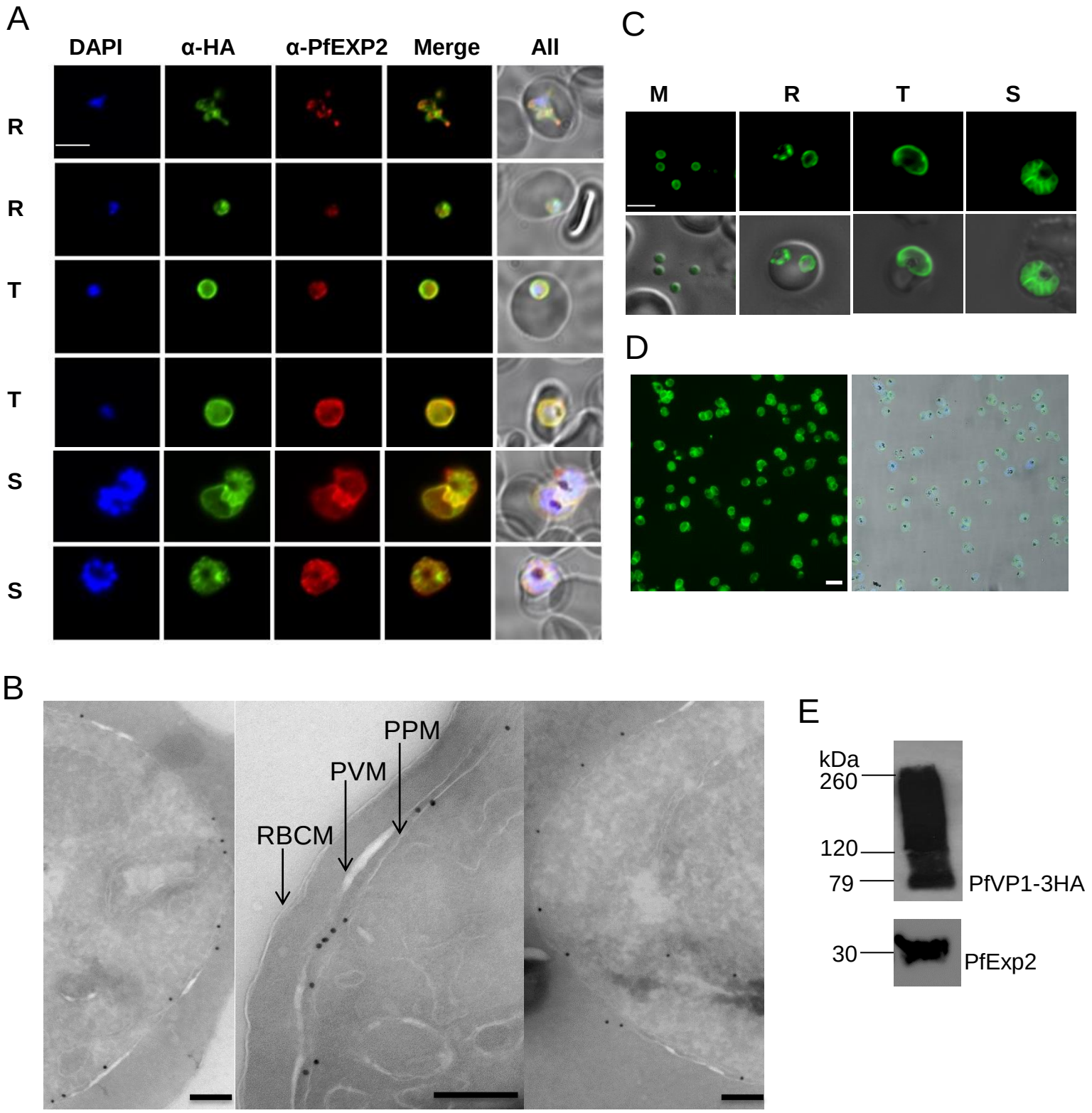

Fig 1. PfVP1 is mainly localized to the parasite plasma membrane

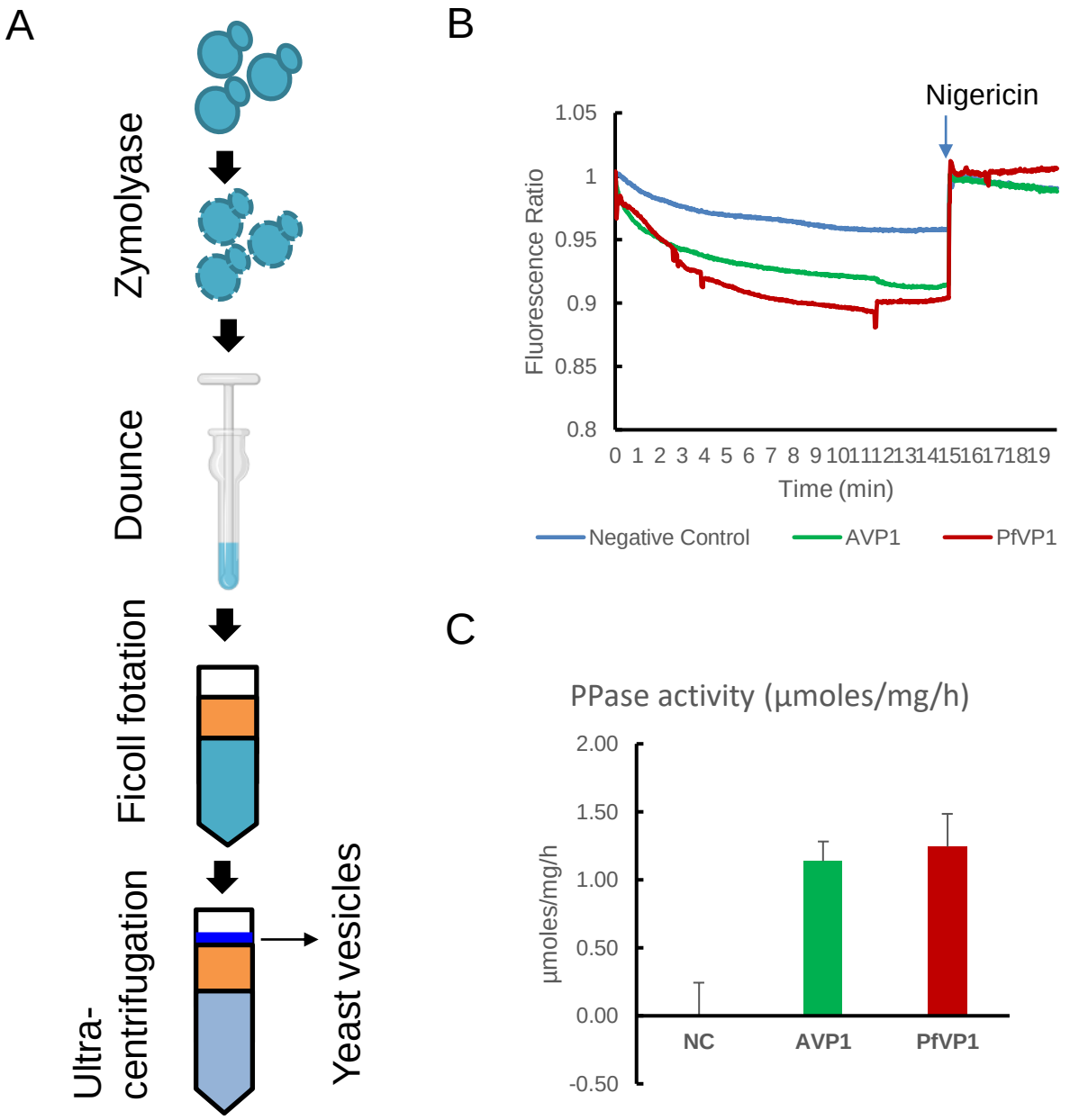

Figure 2. PfVP1 is a PPi hydrolyzing proton pump

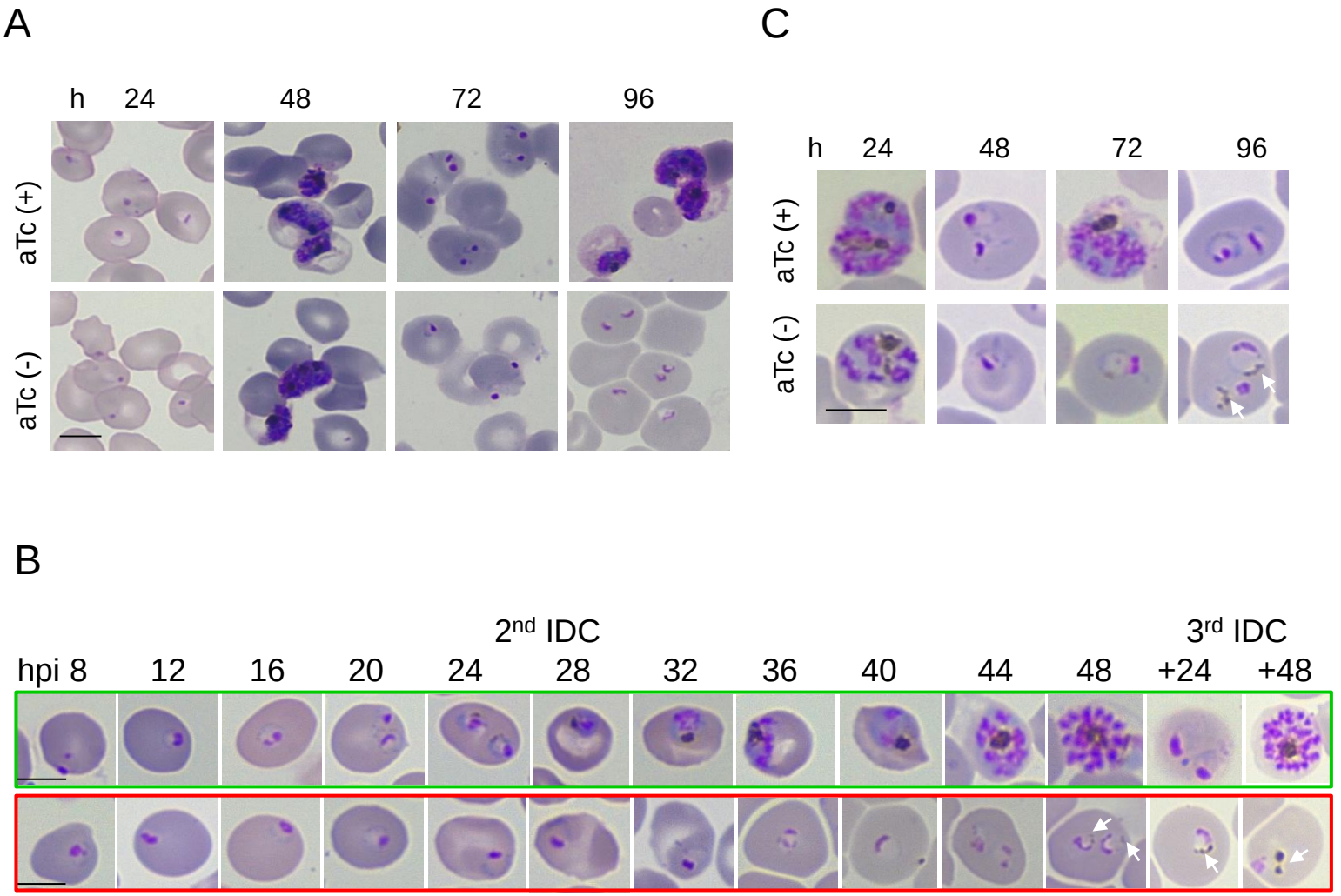

Fig 3. PfVP1 is essential for the ring to trophozoite transition

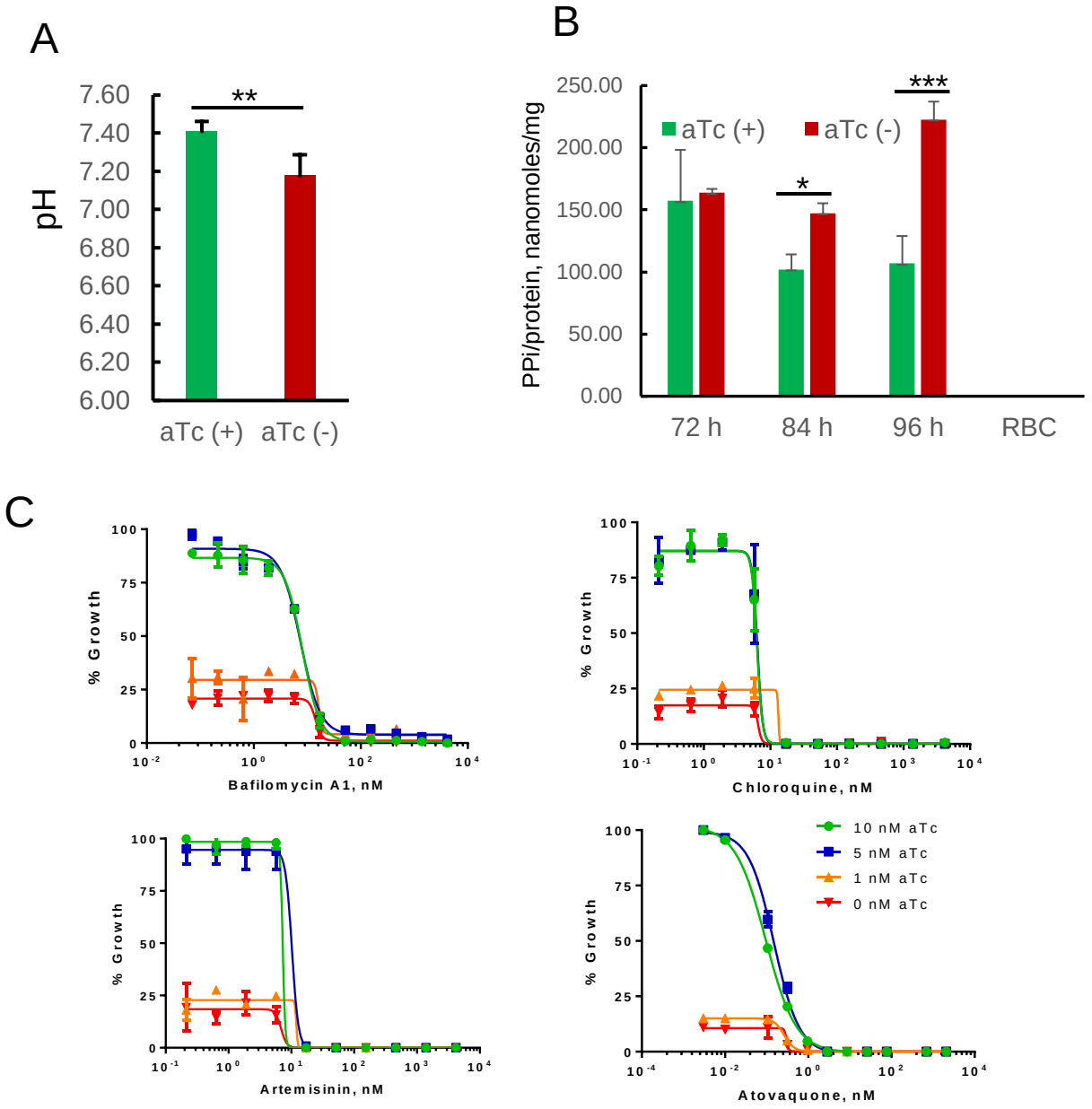

Fig 4. Phenotypic characterization of the PfVP1 knockdown parasite

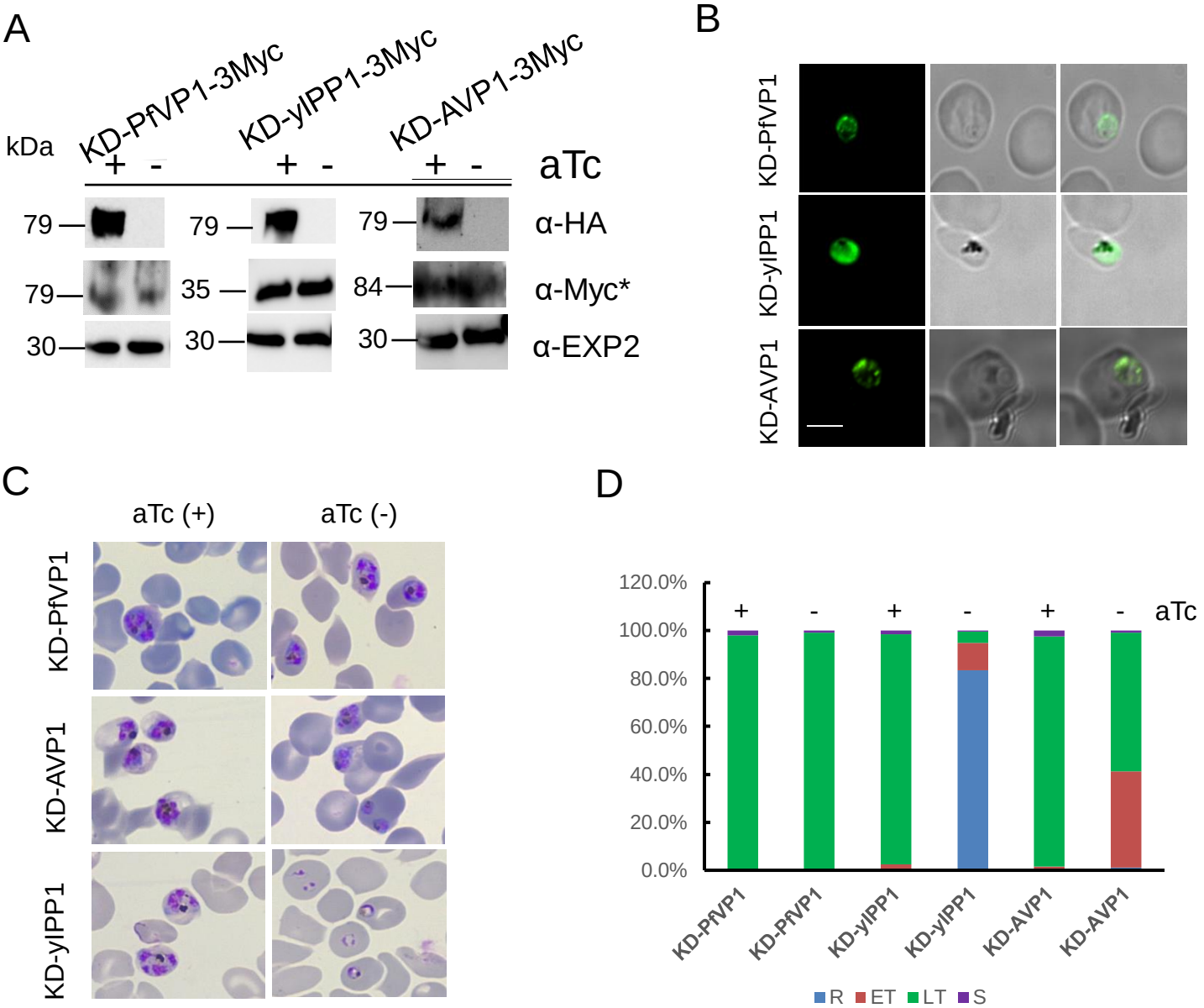

Fig 5. The dual functionality of PfVP1 is required for parasite survival

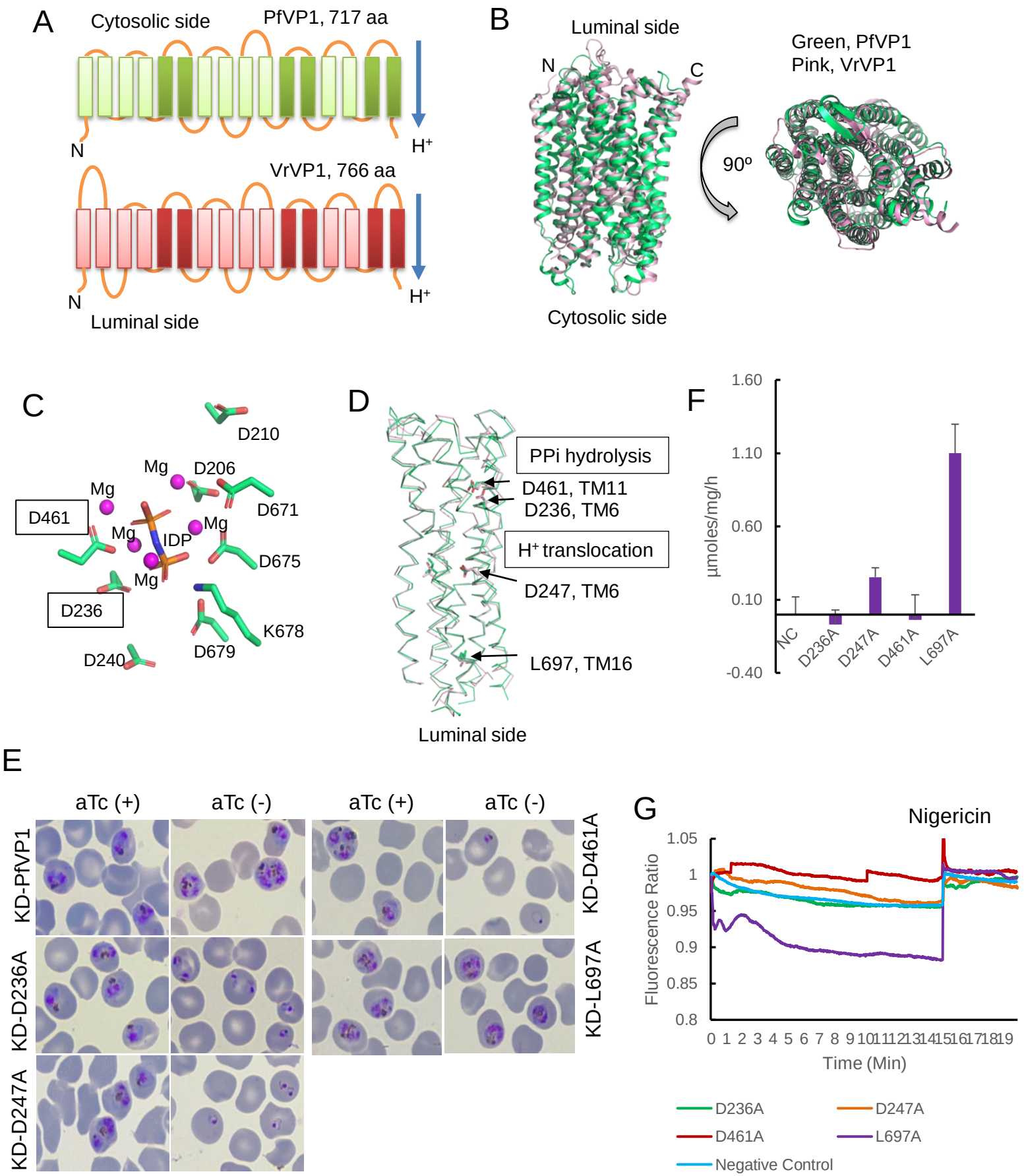

Fig 6. Structure guided mutagenesis analysis of PfVP1